OPEN

Citation: Cell Death and Disease (2013) 4, e670; doi:10.1038/cddis.2013.201

www.nature.com/cddis

Alterations in c-Myc phenotypes resulting from dynamin-related protein 1 (Drp1)-mediated mitochondrial fission

M Sarin[1], Y Wang[2], F Zhang[1], K Rothermund[1], Y Zhang[2], J Lu[1], S Sims-Lucas[3], D Beer-Stolz[4], BE Van Houten[5,6], J Vockley[2], ES Goetzman[2], J Anthony Graves[1] and EV Prochownik*[,1,5,7]

The c-Myc (Myc) oncoprotein regulates numerous phenotypes pertaining to cell mass, survival and metabolism. Glycolysis, oxidative phosphorylation (OXPHOS) and mitochondrial biogenesis are positively controlled by Myc, with *myc*−/− rat fibroblasts displaying atrophic mitochondria, structural and functional defects in electron transport chain (ETC) components, compromised OXPHOS and ATP depletion. However, while Myc influences mitochondrial structure and function, it is not clear to what extent the reverse is true. To test this, we induced a state of mitochondrial hyper-fission in rat fibroblasts by de-regulating Drp1, a dynamin-like GTPase that participates in the terminal fission process. The mitochondria from these cells showed reduced mass and interconnectivity, a paucity of cristae, a marked reduction in OXPHOS and structural and functional defects in ETC Complexes I and V. High rates of abortive mitochondrial fusion were observed, likely reflecting ongoing, but ultimately futile, attempts to normalize mitochondrial mass. Cellular consequences included reduction of cell volume, ATP depletion and activation of AMP-dependent protein kinase. In response to Myc deregulation, apoptosis was significantly impaired both in the absence and presence of serum, although this could be reversed by increasing ATP levels by pharmacologic means. The current work demonstrates that enforced mitochondrial fission closely recapitulates a state of Myc deficiency and that mitochondrial integrity and function can affect Myc-regulated cellular behaviors. The low intracellular ATP levels that are frequently seen in some tumors as a result of inadequate vascular perfusion could favor tumor survival by countering the pro-apoptotic tendencies of Myc overexpression.

Cell Death and Disease (2013) **4,** e670; doi:10.1038/cddis.2013.201; published online 13 June 2013
Subject Category: Cancer Metabolism

Many human cancers demonstrate de-regulation of the c-Myc (Myc) oncoprotein, a bHLH-ZIP (basic helix-loop-helix-leucine zipper) transcription factor that modulates genes transcribed by all three RNA polymerases.[1,2] Among Myc's targets are genes whose products regulate metabolism, including enzymes involved in glycolysis and oxidative phosphorylation (OXPHOS).[3–5] This property likely accounts for Myc's capacity to promote the Warburg effect, which is defined as the generation of ATP via glycolysis despite sufficient oxygen to support OXPHOS.[5,6] However, the Warburg effect and OXPHOS are not mutually exclusive activities, and both glycolysis and OXPHOS are increased and de-regulated in Myc overexpressing cells.[4,7,8] It is likely that these processes represent different facets of the flexible metabolic state that supports the high rates of proliferation and anabolism of transformed cells.[5,9,10] By providing for the rapid but inefficient generation of ATP, glycolysis also promotes tumor survival in hypoxic environments generated by inadequate vascular perfusion.[5,9,11]

Additional Myc target genes include those involved in mitochondrial and ribosomal biogenesis, biomass accumulation and survival.[2,4,12] Mitochondrial mass and interconnectivity, cellular mass and protein synthetic rates are increased by aberrant Myc expression, whereas the opposite occurs in *myc*−/− cells.[4,13–15] Myc ablation is also associated with ATP depletion that likely arises from a combination of atrophic mitochondria, reduced glycolysis and OXPHOS and electron transport chain (ETC) dysfunction.[4] Myc's role in survival

[1]Division of Hematology/Oncology, Children's Hospital of Pittburgh of UPMC, Pittsburgh, PA, USA; [2]Division of Medical Genetics, Children's Hospital of Pittburgh of UPMC, Pittsburgh, PA, USA; [3]Division of Nephrology, Children's Hospital of Pittsburgh of UPMC, Pittsburgh, PA, USA; [4]Center for Biological Imaging, The University of Pittsburgh, Pittsburgh, PA, USA; [5]The University of Pittsburgh Cancer Institute, Pittsburgh, PA, USA; [6]The Department of Pharmacology and Chemical Biology, The University of Pittsburgh Medical Center, Pittsburgh, PA, USA and [7]Department of Microbiology and Molecular Genetics, The University of Pittsburgh Medical Center, Pittsburgh, PA, USA
*Corresponding author: EV Prochownik, Section of Hematology/Oncology, Rangos Research Center, Room 5124, Children's Hospital of Pittsburgh of UPMC, 4401 Penn Avenue, Pittsburgh, PA 15224, USA. Tel: (412) 692-6795; Fax: (412) 692-5228; E-mail: procev@chp.edu
Keywords: apoptosis; glycolysis; mitofusins; OXPHOS; Warburg effect
Abbreviations: AICAR, 5-amino-1-β-D-ribofuranosyl-imidazole-4-carboxamide; AMPK, AMP-dependent protein kinase; AUC, area under the curve; CM-H2DCFDA, chloromethyl derivative of 2′,7′-dichlorodihydrofluorescein diacetate; BNGE, blue-native gel electrophoresis; CHX, cycloheximide; DMEM, Dulbecco's modified Eagle's minimal essential medium; Drp1, dynamin-related protein 1; DsRED-mito, *Discosoma* sp. red fluorescent protein fused to a mitochondrial signal peptide; 2-DG, 2-deoxyglucose; ECAR, extracellular acidification rate; EGFP-Mito, enhanced green fluorescent protein fused to a mitochondrial localization signal; ETC, electron transport chain; FCCP, cyanide p-trifluoromethoxy-phenylhydrazone; MycER, human Myc protein fused to the estrogen receptor hormone-binding domain; NAO, 10-nonoyl-acridine orange; OXPHOS, oxidative phosphorylation; OCR, oxygen consumption rate; PEG, polyethylene glycol; ROS, reactive oxygen species
Received 09.4.13; revised 07.5.13; accepted 10.5.13; Edited by G Raschellà

involves both intrinsic and extrinsic apoptotic pathways, which converge at the mitochondrial level.[16] For example, Myc activates certain pro-apoptotic members of the Bcl-2 family such as Bax and Bim and suppresses anti-apoptotic members, such as Bcl2 itself and Bcl-X_L.[16] Highly coordinated interactions among these members are needed to ensure maximal control over these survival pathways.[16]

Mitochondria normally engage in a dynamic interplay between fusion into large, interconnected reticular networks and fission, which produces smaller, fragmented organelles.[17–19] Fusion is believed to improve respiration and prolong organelle lifespan by limiting the oxidation of mitochondrial contents as a result of their dilution with the undamaged molecules of larger and healthier organelles.[17,18] By contrast, fission reduces mitochondrial mass during periods of relative metabolic inactivity and aids in the removal of dysfunctional organelles.[17–19,20] Because of varying degrees of fitness among mitochondria at either end of the fission–fusion spectrum, these activities can exert significant effects on cell survival.[17,21,22]

The balance between fission and fusion is orchestrated by a group of proteins that localize to the outer or inner mitochondrial membrane.[17–19] Among the major mammalian fission proteins, dynamin-related protein 1 (Drp1) has additional roles in maintaining mitochondrial shape, size, distribution and cristae remodeling.[17,22–25] Purified Drp1 spontaneously forms oligomeric ring-like structures *in vitro* and reversibly localizes to sites of mitochondrial constriction during fission.[26] These sites are also encircled by projections of endoplasmic reticulum that co-localize with Drp1, promote further contraction and lead to eventual mitochondrial scission.[27]

We have examined here how compromising the normal fission:fusion balance affects Myc's ability to regulate metabolism and energy generation, cell size and survival. We show that constitutive Drp1 overexpression leads to a state of chronic, abortive mitochondrial hyperfission. These mitochondria structurally resemble those of *myc*$-/-$ cells as do their dysfunctional OXPHOS and ETC profiles.[4] Moreover, profound ATP depletion, also resembling that of *myc*$-/-$ cells, likely explains the reduced cell mass and resistance to both Myc-dependent and Myc-independent apoptosis. These results underscore the necessity for maintaining normal mitochondrial dynamics and function in order for Myc to regulate several of its fundamental phenotypes. They suggest that ATP depletion protects cells from the highly pro-apoptotic consequences of Myc de-regulation, thus favoring the survival of tumor cells, particularly when nutrients and/or oxygen are limiting.

Results

Cell line characterization. Rat1a fibroblasts expressing a MycER (human Myc protein fused to the estrogen receptor hormone-binding domain) fusion protein[28] were engineered to express stably a V5-epitope-tagged Drp1 protein (Drp1 cells) or the empty lentiviral vector alone (Vector cells) (Figure 1a). Staining with MitoTracker Green or 10-nonoyl-acridine orange (NAO) showed the mitochondrial mass of pooled Drp1 cells to be approximately half that of Vector cells (Figure 1b). These results were confirmed by stably expressing a *Discosoma* sp. red fluorescent protein fused to a mitochondrial signal peptide (DsRED-Mito). Confocal microscopy and flow cytometry also showed Drp1 cell mitochondrial mass to be reduced (Figure 1c and Supplementary Video S1). On average, these mitochondria were also smaller, less well connected than those of Vector cells and less clustered around the nuclear periphery as previously described in *myc*$-/-$ cells.[4] Enforced Drp1 expression is therefore sufficient to drive a reduction in overall mitochondrial mass and interconnectivity in Rat1a-MycER cells.

Transmission electron microscopy confirmed that in contrast to the mitochondria of Vector cells those of Drp1 cells were smaller, less abundant, less well interconnected and contained a paucity of cristae (Figure 2a). These findings indicate that Drp1 deregulation leads to atrophic mitochondria incapable of forming highly interconnected networks. Moreover, these cumulative deficits lead to an uncompensated reduction in mitochondrial mass. In keeping with these findings, a comparison of several representative mitochondrial membrane and matrix proteins indicated that their levels in Drp1 cells were somewhat reduced (Figures 2b and c).

To appreciate the dynamics of mitochondrial fission and fusion, we co-cultured DsRed2-Mito expressing Vector and Drp1 cells with identical cells expressing mitochondrial-localized enhanced green fluorescent protein (EGFP-Mito) and then induced plasma membrane fusion with polyethylene glycol (PEG). After fixation, heterokaryons expressing both DsRed2-Mito and EGFP-Mito were visualized for evidence of mitochondrial fusion by quantifying the co-localized red and green signals.[4] As shown in Figure 2d, Drp1 cells showed a nearly 15-fold higher rate of mitochondrial fusion. These findings were confirmed and extended by concurrent live cell, confocal, time-lapse imaging of Vector and Drp1 cells stained with MitoTracker Green (Supplementary Video S2). To a greater degree than could be appreciated with the above PEG fusion studies, these experiments also revealed a much more dynamic population of mitochondria in the latter cells, even among those organelles not undergoing fission or fusion. Collectively, these results indicate that, despite their structural defects, Drp1 cell mitochondria are more actively engaged in fusion. However, the newly fused organelles appear to be unstable and subject to immediate *de novo* fission.

Structural and functional abnormalities in ETC components in Drp1 cells. Because the properties of Drp1 cell mitochondria were reminiscent of those from *myc*$-/-$ rat fibroblasts,[4,15,29] we compared the four mitochondrial ETC components plus Complex V (ATP synthase) in Vector and Drp1 cells using blue-native gel electrophoresis (BNGE).[30,31] Supercomplexes, comprised of Complexes I, III and IV[30] and possessing higher intrinsic Complex I activity, can also be visualized by this method.[4] As shown in Figure 3a, BNGE of mitochondria from Vector cells resolved each of the ETCs in proportions roughly equivalent to those we previously described for another strain of *myc*$+/+$ rat fibroblasts.[4] By contrast, the BNGE profile of Drp1 mitochondria was strikingly different. Quantification of these differences

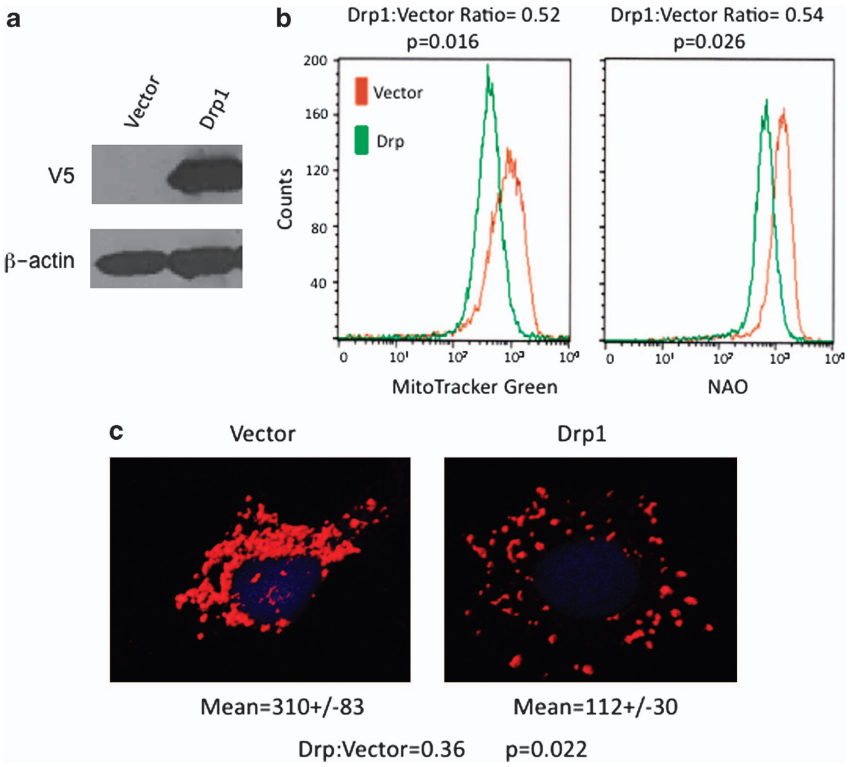

Figure 1 Characterization of cell lines and mitochondria. (**a**) Stable expression of Drp1. Rat1a MycER cells were stably transduced with a lentiviral vector encoding a full-length, rat Drp1-V5 fusion protein (Drp1 cells) or with the empty parental vector (Vector cells). Drp1 protein expression was assessed by immunoblotting for V5 epitope expression. (**b**) Quantification of mitochondrial mass. Cell lines were evaluated by flow cytometry after staining with MitoTracker Green or NAO to quantify overall mitochondrial mass. Drp1:Vector mean fluorescence ratios are expressed above each flow histogram. The results shown are typical of at least 4–6 independent experiments performed at different times. (**c**) Representative confocal images obtained on cells stably transfected with a plasmid encoding DsRED2-Mito. Mean fluorescence intensities were also quantified by flow cytometry with the Drp1:Vector ratio being shown beneath the panel. See Supplementary Video S1 for additional images

(Figure 3b) showed significant reductions in Complex V (45%) and supercomplexes (38%). By contrast, Complexes II, III and IV were unaffected, whereas Complex I was reduced by 28%, although this did not reach statistical significance. A previously uncharacterized complex (Complex 'X'), originally seen in mitochondria of *myc*−/− cells and shown to contain >40 subunits of Complexes II–V,[4] was also increased by approximately twofold in Drp1 cells. Thus, Drp1 cell mitochondria contain abnormalities in supercomplexes, Complex V and Complex X, that closely resemble those of *myc*−/− cells.

To investigate the significance of the above quantitative differences in ETC components, we performed *in situ* enzymatic activity assays for complexes I and V using the same gels used for BNGE determinations.[4] Both the NADH ubiquinone oxidoreductase activity of Complex I and its associated supercomplexes (Figures 4a and b) and the ATPase activity of Complex V (Figures 4c and d) were significantly reduced in Drp1 cells. In addition, the presence of a Complex V component, termed F1, which is believed to reflect Complex V dysfunction,[32,33] was increased in Drp1 cells, although this did not reach statistical significance ($P=0.07$; Figures 4 c and d). That the activities of Complex I and supercomplexes in Drp1 cells are reduced out of proportion to their actual levels as measured by BNGE suggests that these complexes are dysfunctional.

Metabolic defects in Drp1 cells and their consequences. To determine whether the above-described defects also affected mitochondrial metabolism, we measured oxygen consumption rates (OCRs) in Vector and Drp1 cells as a way of assessing OXPHOS. We also quantified glycolysis in the same samples by measuring the extracellular acidification rate (ECAR). As seen in Figure 5a, the basal OCR of Vector cells, measured during the first 30 min of the experiment, was more than twice that of Drp1 cells ($P<0.001$), thus closely mirroring the differences in the total mitochondrial mass described in Figures 1b and c and Supplementary Video S1. The subsequent addition of various metabolic inhibitors[4,7] showed responses that were largely attenuated in Drp1 cells. For example, we noted that the level of ATP-linked respiration, that is, the difference in the basal rate of OCR minus that following the addition of oligomycin, was approximately twofold lower in Drp1 cells. Additionally, both the maximal respiratory rate and the spare respiratory capacity of Vector cells, defined as the total area under the curve (AUC) between the addition of cyanide p-trifluoromethoxy-phenylhydrazone (FCCP) and 2-deoxyglucose (2-DG) and the same AUC minus basal respiration, respectively,[34–36] were also significantly attenuated in Drp1 cells. Concurrent measurements showed that basal levels of ECAR were also reduced in Drp1 cells by over twofold, thus mirroring our findings with OCR (Figure 5b). Collectively,

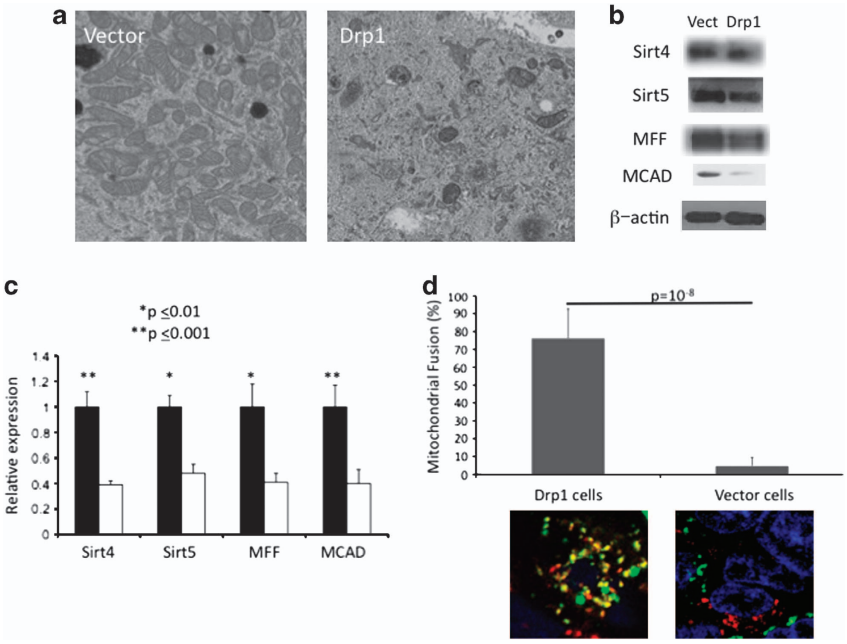

Figure 2 Abnormal mitochondrial ultrastructure and mitochondrial fusion of Drp1 cells. (**a**) Transmission electron micrographs of Vector and Drp1 cells showing a high degree of mitochondrial interconnectivity and abundant, well-organized cristae patterns in the former cells and small, sparse mitochondria with a lack of interconnectivity and poorly formed cristae in the latter cells. (**b**) Immunoblotting for select mitochondrial membrane and matrix proteins in Vector and Drp1 cells. Proteins included sirtuins (sirt) 3 and 5, mitochondrial fission factor (MFF) and medium-chain acyl-CoA-dehydrogenase (MCAD). Typical results are depicted. (**c**) Quantification of the western blots shown in panel (**b**). Three separate immunoblots typical of those depicted in panel (**b**) were densitometrically scanned and normalized to β-actin. The values obtained for Vector cells were then arbitrarily set to 1. The results of relative mean band intensities $\pm$ 1 S.E. are shown. (**d**) Higher rates of mitochondria fusion in Drp1 cells. Vector and Drp1 cells stably expressing DsRed2-Mito or EGFP-Mito were mixed in equal numbers and fused with PEG for 1 min. After washing, cells were incubated in medium containing CHX for 2 h, fixed, stained with DAPI and examined by confocal microscopy. Mitochondrial fusion in the resultant heterokaryons was identified by the merging of green and red signals. The histogram indicates the degree of mitochondrial fusion in each cell pair and was generated by calculating the percentage of co-localized fluorescent signals from at least 20 randomly selected heterokaryons with the use of the CoLocalizer Pro software package. Fluorescence micrographs below the histogram show typical images of mitochondrial fusion in each cell type. The rapidly alternating fission and fusion activity in the Drp1 cells when compared with the Vector cells can best be appreciated in the time-lapse movies in Supplementary Video S2

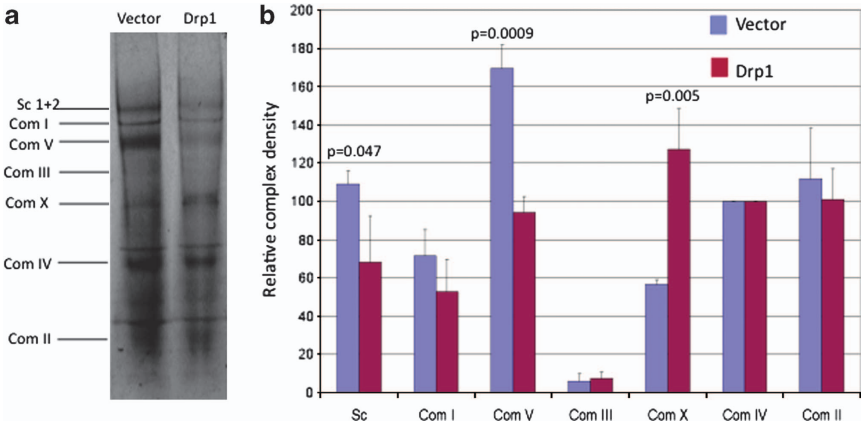

Figure 3 Aberrant ETC complexes in Drp1 cells. (**a**) BNGE of purified mitochondria from Vector and Drp1 cells. Each of the major complexes and supercomplexes (SC) is indicated. (**b**) Quantification of ETC differences in Vector and Drp1 cells. Complex abundance was determined by scanning densitometry of Coomassie blue-stained blue-native gels similar to those depicted in panel **a** and arbitrarily expressed relative to Complex IV, which showed no change between the two cell lines. An aberrant complex (Complex 'X'), previously seen in *myc*$-/-$ cells[4] was also observed at a significantly elevated level in Drp1 cells

these findings were consistent with the subsequent documentation of a state of severe ATP depletion in Drp1 cells (Figure 5c).

Reduced ATP levels are generally countered by the phosphorylation-dependent activation of the α-subunit of AMP-dependent protein kinase (AMPK), an energy-sensing enzyme that normalizes ATP levels by tempering anabolic reactions while coordinately increasing glucose uptake and fatty acid β-oxidation.[37] As expected, pAMPK levels were markedly elevated in Drp1 cells, indicating that, while this

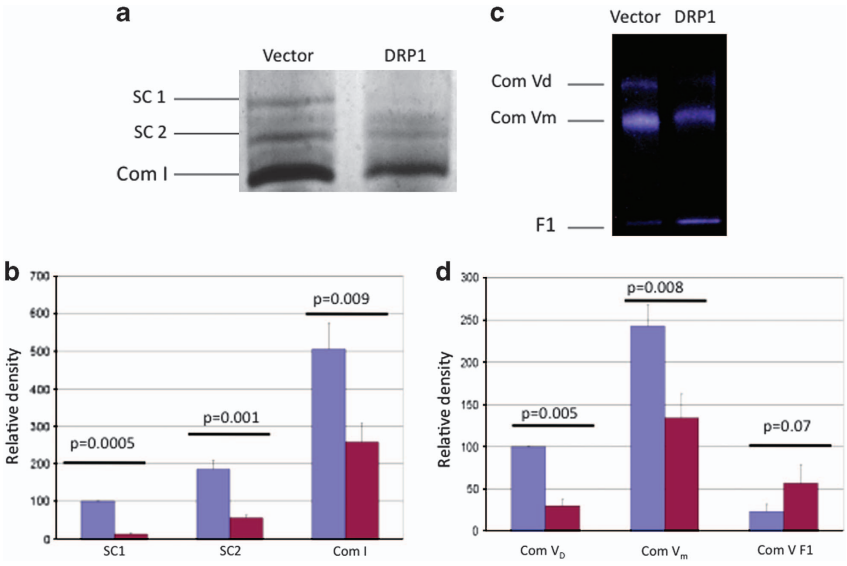

Figure 4 Abnormal *in situ* ETC complex activities in Drp1 cells. (**a**) Complex I activity. *In situ* staining for NADPH (nicotinamide adenine dinucleotide phosphate reduced) ubiquinone oxidase was performed as previously described[6] with gels similar to those shown in panel (**a**). A typical result is shown. (**b**) Quantification of the results shown in panel (**a**). The mean values of three independent *in situ* determinations are shown ± 1 S.E. Note the better resolution of the individual components of the supercomplexes (SC1 and SC2) than is seen in panel (**a**). (**c**) Complex V activity. *In situ* ATPase activity was determined as previously described[6] using the same gels used to quantify Complex I activities. (**d**) Quantification of the results shown in panel (**c**). The mean values ± 1 S.E. of three independent *in situ* determinations are shown

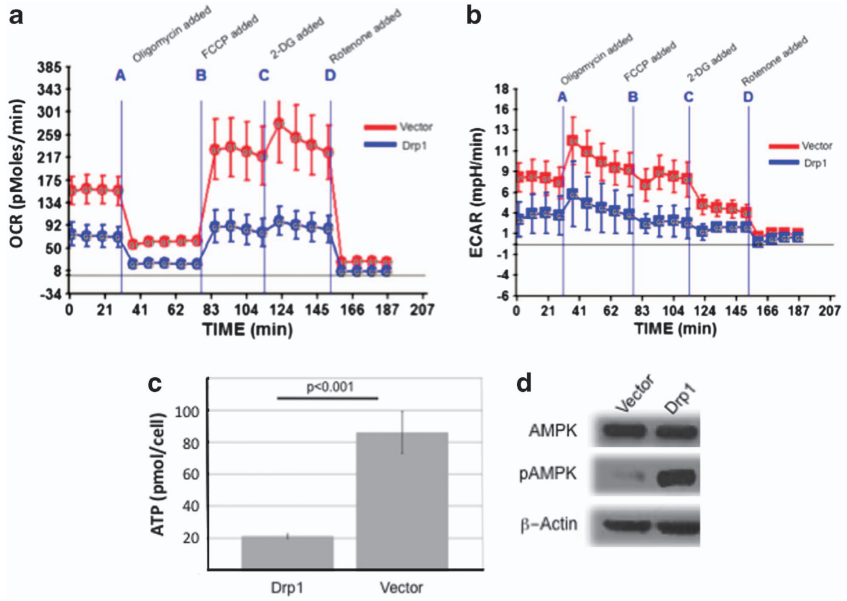

Figure 5 Metabolic abnormalities in Drp1 cells. (**a**) Quantification of OXPHOS. Vector and Drp1 cells were analyzed in parallel using a Metabolic Flux Analyzer as previously described.[4] Note the higher basal OCR in vector cells as measured between 0 and 30 min ($P<0.001$). The addition of specific metabolic inhibitors at various times is indicated. (**b**) Quantification of glycolysis. ECAR was measured on the same samples used to quantify OCR in panel (**a**). Basal rates were significantly higher in Vector cells ($P<0.001$). (**c**) Severe depletion of ATP in Drp1 cells. ATP levels were determined as previously described[4] and are indicated as the mean of quadruplicate samples ± 1S.E. (**d**) Immunoblotting for total AMPK and phospho-AMPK (α-subunit Thr$_{172}$) in Vector and Drp1 cells. β-Actin was included as a protein loading control

pathway was intact and appropriately responsive, its activation was unable to correct the severe energy deficit in the face of ongoing mitochondrial fission (Figure 5d).

ETC dysfunction can lead to free electron loss, primarily via Complex I and Complex III, and a resultant increase in reactive oxygen species (ROS).[30,31,38] This would be consistent with the observed Drp1 cell ETC deficits as well as the marked ATP-depleted state, which by itself can increase ROS.[38] We therefore measured total cellular ROS using CM-H2DCFDA staining and found a nearly twofold increase in Drp1 cells (Figure 6a) that was confirmed using MitoSOX, a dye that measures superoxide, a specific product of OXPHOS[39] (Figure 6b). Indeed, when considered relative to the twofold differences in mitochondrial mass (Figure 1b), the

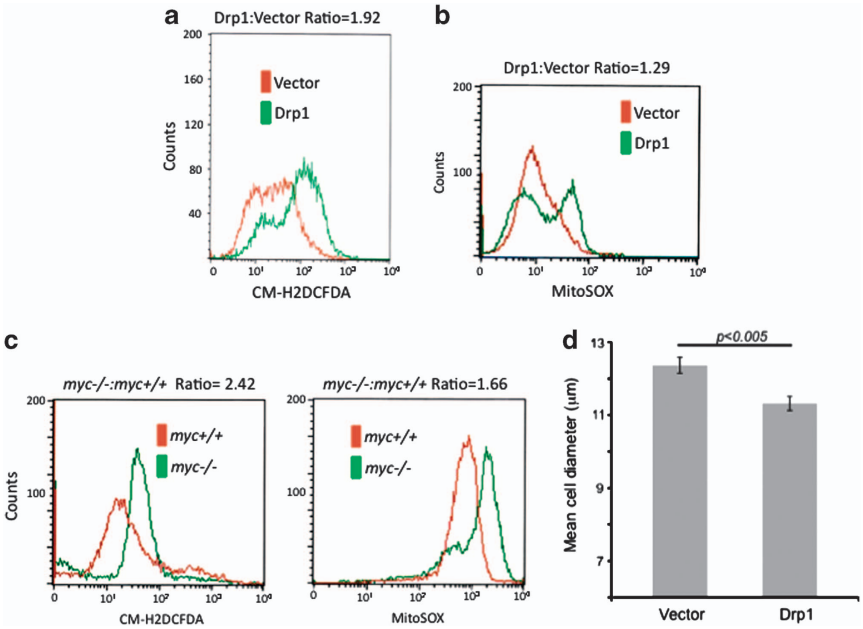

Figure 6 Abnormalities of ROS production by and reduced size of Drp1 cells. (**a**) Measurement of total cellular ROS. Vector and Drp1 cells were exposed to CM-H_2DCFDA as previously described[4,7] and analyzed by flow cytometry. Nearly identical results were observed on three separate occasions (not shown). The ratios of the mean fluorescence are indicated above the panels. (**b**) Measurement of mitochondrial superoxide production using MitoSOX staining in Vector and Drp1 cells. (**c**) ROS production by *myc*+/+ (TGR1) fibroblasts and *myc*−/− rat fibroblasts. Cells were plated and stained with CM-H2DCFDA and MitoSOX as described in panels (**a**) and (**b**). (**d**) Cell size determinations. Vector and Drp1 cells were plated onto 100-mm tissue culture dishes, and grown for two days to allow the maximal proliferative rates to be achieved. The cells from subconfluent confluent plates were then harvested by trypsinization, stained with trypan blue and the diameters of all viable cells were determined on a Beckman-Coulter Vi Cell analyzer. At least five independent cell size determinations were performed at different times with a minimal of 3000 cells per determination. The mean cell diameter ±1 S.E. is shown

ROS production differential between Vector and Drp1 cells was nearly fourfold. Overall, the increase in ROS by Drp1 cells was comparable with that of *myc*−/− rat fibroblasts (Ref. 4 and Figure 6c). These findings indicate that Drp1 cell ETC defects are associated with reduced metabolic function, severe ATP depletion, promiscuous electron leak and ROS generation whose origins can largely be traced to the dysfunctional mitochondria.

The depletion of ATP in Drp1 cells, presumably caused by one or more respiratory chain defects and coupled with an intact but ineffectual pAMPK response, suggested that alternate compensatory mechanisms might be needed to minimize energy consumption while preserving survival and proliferation. One way by which this could be accomplished would be via reduced biomass.[40] Indeed, similar to what we previously observed in *myc*−/− fibroblasts,[4] the overall Volume of Drp1 cells was reduced >30% relative to Vector cells (Figure 6d).

Resistance of Drp1 cells to Myc-mediated apoptosis is ATP-dependent. Rat1a-MycER cells were originally selected for their robust pro-apoptotic response following MycER activation by 4-HT. Consistent with this, Vector cell proliferation was significantly impaired following 4-HT addition, even in the presence of high serum concentrations, due to an increasing apoptotic population (Figure 7a and data not shown). By contrast, Drp1 cells, which grew at nearly the same rate as Vector cells in the absence of 4-HT showed marked apoptotic resistance following Myc activation.

We next monitored the survival of sub-confluent cultures of serum-deprived Vector and Drp1 cells in the absence or presence of 4-HT, thus allowing an assessment of both Myc-dependent and Myc-independent apoptosis. As expected,[7,41,42] Vector cells rapidly succumbed following serum removal, particularly when combined with Myc activation (Figure 7b). By contrast, a greater fraction of Drp1 cells survived under both conditions. These results were supported by studies of cytochrome *c* release, the inciting event in the intrinsic apoptotic pathway.[16,43] Consistent with their higher sensitivity to Myc-induced apoptosis, mitochondrial cytochrome *c* release and its cytoplasmic accumulation occurred much more rapidly in Vector cells than in Drp1 cells. Taken together, these results indicate that Drp1 inhibits both Myc-dependent and Myc-independent apoptotic responses.

Because several key steps in both the intrinsic and extrinsic apoptotic pathways are ATP-dependent,[44,45] we next asked whether Drp1 cell survival could be attributable to their ATP-depleted state (Figure 5b). We therefore exposed Drp1 cells to 5-amino-1-β-D-ribofuranosyl-imidazole-4-carboxamide (AICAR), an AMP analog that increases ATP levels by activating AMPK and increasing OXPHOS.[37,46] As seen in Figure 8a, exposure of Drp1 cells to AICAR for as little as 4 h led to over twofold increases in ATP and pAMPK levels (Figure 8b). We then assessed Drp1 cell survival after activating Myc in the absence or presence of AICAR. As seen in Figures 8c, 4-HT alone only modestly reduced survival, thus confirming our previous findings (Figure 7a). Although AICAR alone reduced survival modestly, the

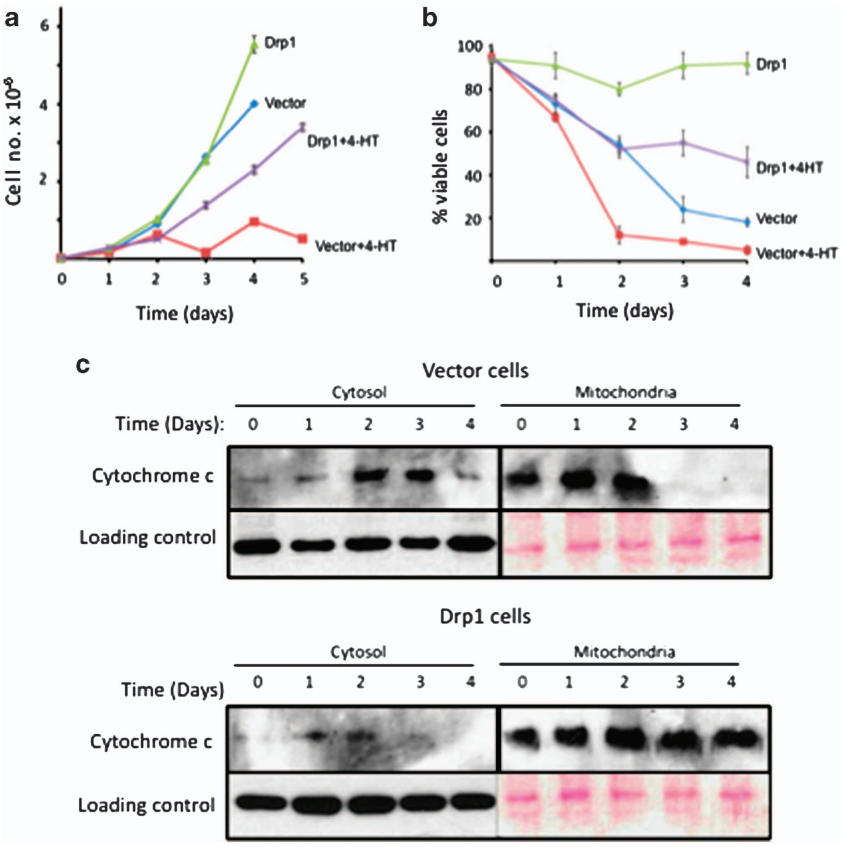

Figure 7 Drp1 cells are resistant to apoptotic signals. (**a**) Growth curves. In all, 10^5 Vector and Drp1 cells were seeded onto 100-mm tissue culture plates in growth medium containing 10% fetal bovine serum and allowed to attach overnight. The following day (day 0), cells were counted and fresh growth medium either lacking or containing 4-HT was then added. Viable cell counts were then performed daily using a Vi-Cell analyzer. The results shown represent the mean of triplicate determinations $\pm$ 1 S.E. (**b**) Apoptosis profiles. Vector and Drp1 cells were seeded onto 100-mm plates in growth medium and allowed to achieve $\sim$80% confluency at which point (day 0) the total number of viable cells was determined from triplicate cultures. The remaining monolayers were then maintained for the duration of the experiment in serum-free medium either lacking or containing 4-HT, and the number of viable cells was determined daily thereafter. (**c**) Delayed cytochrome *c* release from Drp1 cells. Cells were initially plated and grown as described in panel (**b**) and then deprived of serum upon reaching $\sim$80% confluency. At the indicated time points, the cells were harvested and fractionated into cytosolic and mitochondrial fractions. Immunoblotting was then performed to allow for detection of cytochrome *c* release from the mitochondria. Loading controls consisted of β-actin for cytosolic fractions and Ponceau Red staining of the low molecular weight region of the membrane corresponding to the region of cytochrome *c* migration

combination of Myc activation and AICAR produced a much more pronounced reduction in survival. Moreover, continuous AICAR exposure normalized Drp1 cell size (Figure 8d). Thus, we conclude that AICAR increases ATP levels in Drp1 cells, sensitizes them to Myc-induced apoptosis and increases mean cell volume.

Discussion

Mitochondria typically participate in fission, fusion and remodeling in response to stress and metabolic change.[17,18] The balance among these activities is maintained by the fission/fusion protein family, including Drp1.[17,18,23–25] A role for Drp1 in apoptosis has also been proposed,[47–49] and both its overexpression and inhibition can influence survival in complex ways that are dependent on the cell type, the inciting apoptotic trigger and possibly the nature of the Drp1 isoform that is perturbed.[22,23,26,37,48–50] Fission is an early apoptotic event[18,48,51] and is often coordinated with the activation of pro-apoptotic Bcl-2 family member proteins such as Bax, which leads to outer membrane permeabilization, cytochrome *c* release and the collapse of mitochondrial outer membrane potential.[26,47,48] However, it has not been determined whether fission itself has a causal role in apoptosis or simply reflects the consequences of downstream processes that initiate cell death. Our results indicate that forced Drp1-mediated mitochondrial fission alone is insufficient to enhance apoptosis and indeed has precisely the opposite effect when cells are serum-deprived and/or when Myc is overexpressed.

It is likely that the common metabolic profiles of Drp1 and *myc*$-/-$ cells, namely attenuated OXPHOS, ATP depletion and increased ROS generation, reflect the similarities in their ETC defects.[4] This suggests that they are a generic response to impaired mitochondrial fusion, irrespective of its cause. Complex I defects are known to promote electron loss,[31,52] thus potentially explaining the higher ROS production by Drp1 cells described here (Figures 4c and d). Moreover, unlike *myc*$-/-$ cells, where quantitative and qualitative reductions in Complex I occur in parallel,[4] the functional defects of Complex I in Drp1 cells are disproportionate to the levels documented by BNGE. This suggests that Drp1 may alter Complex I activity without necessarily affecting its BNGE

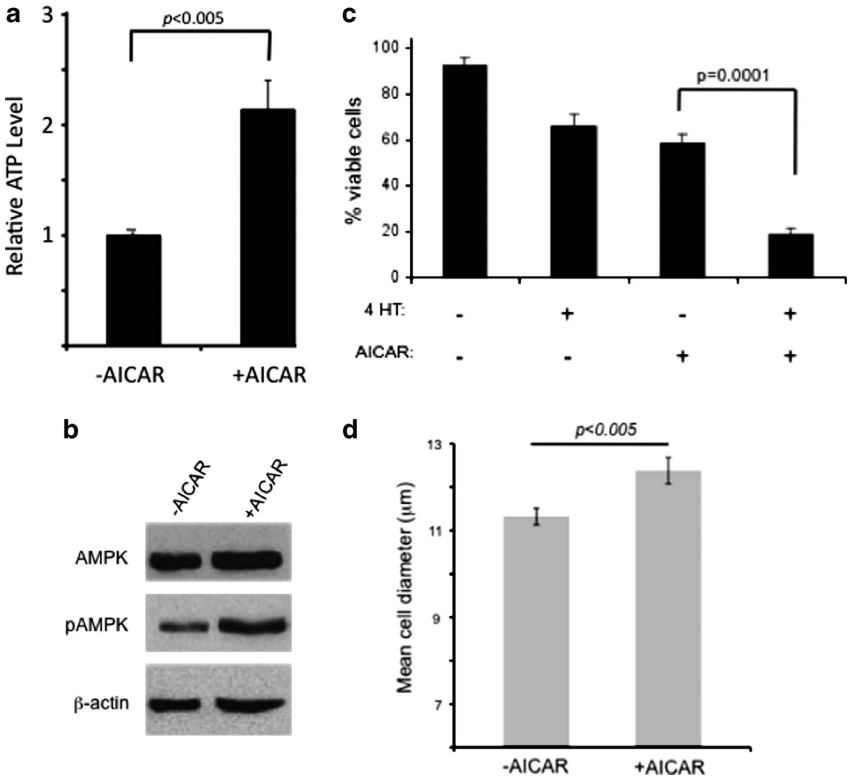

Figure 8 AICAR restores ATP levels in Drp1 cells and accelerates Myc-dependent apoptosis. (**a**) Drp1 cells were seeded in 96-well plates as described for Figure 5b. The following day, fresh medium containing 250 μM AICAR or vehicle alone was added and ATP levels were determined 4 h later. The histogram shows the mean relative ATP levels ± 1 S.E. from quadruplicate samples. (**b**) Parallel cultures of cells, maintained in 100-mm plates, were treated as described in panel (**a**) and were evaluated by immunoblotting for total and pAMPK levels. In Drp1 cells, the levels of pAMPK relative to total AMPK levels were 2.5-fold higher compared with Vector cells. (**c**) Drp1 cells were maintained under standard growth conditions (Figure 6a) for 3 days in the presence or absence of 4-HT and 250 μM AICAR. The total number of viable cells was then determined. The results are expressed as the mean of triplicate sets of cultures ± 1 S.E. (**d**) Changes in the mean diameter of Drp1 cells following a 3-day exposure to AICAR. Cells were maintained and counted as described in Figure 6d. The results represent the mean diameters ± 1 S.E. of at least 3000 cells from triplicate cultures

profile. Together with significantly lowered activity of complex V and reduced overall mitochondrial mass, such abnormalities likely account for the severely ATP-depleted states of Drp1 and *myc*−/− cells.

One property that does distinguish the mitochondria of Drp1 cells is their excessive rate of abortive fusion (Figure 2b and Supplementary Video S2). Given that Myc-replete Drp1 cells proliferate more rapidly than *myc*−/− cells,[29] they may be under greater pressure to maximize ATP production even though basal levels in both the cells are comparable (Ref. [4] and Figure 5c). Because ectopic Drp1 limits increases in mitochondrial mass and function that would otherwise be needed under such circumstances, the high rates of abortive fusion may represent a compensatory, albeit ultimately futile, attempt to normalize OXPHOS and ATP. Another possibility is that Drp1 overexpression enhances fusion via non-energy-sensing pathways.[19] That comparable rates of mitochondrial fusion do not occur in *myc*−/− cells may reflect the absence of Myc expression itself and its effects on mitochondrial biogenesis[6,24] and/or their greatly reduced proliferative rate and lower ATP requirements.[4] Myc may also regulate fission and fusion proteins other than Drp1 that promote the high fusion rate of Drp1 cells.[4] At the very least, our findings indicate that, despite their importance, mitochondrial size and integrity are not the only factors that coordinate fission and fusion processes.

Because Myc influences numerous functions,[2,53] it is not surprising that *myc*−/− cells possess a broader range of phenotypes than Drp1 cells. However, the latter's behavior suggests that at least some of the *myc*−/− cell phenotypes are indirect and the result of a state that favors permanent mitochondrial fission and or atrophy. This interpretation may be subject to further refinement given that certain cell types in which fusion is compromised as a result of mitofusion 2 (*mfn2*) deletion show less impressive changes in mitochondrial ultrastructure than those described here and are actually somewhat larger than their *mfn2*+/+ counterparts.[54]

We do not currently understand the precise means by which Drp1 affects mitochondrial phenotype. Possible influences include the identity of the expressed isoform, its subcellular distribution and/or its post-translational regulation by phosphorylation, ubiquitinylation and/or sumoylation.[55] Drp1 can affect cristae structure[47] and may even have a role in mitochondrial fusion, all of which could be differentially affected by such post-translational modifications.[19] These findings are also consistent with the fact that only modest changes in mitochondrial fission and fusion proteins, including Drp1, occur in response to Myc's absence or overexpression.[4]

The apoptotic resistance of Drp1 cells in the presence and absence of serum (Figure 7b) indicates that both Myc-dependent and Myc-independent processes require normal mitochondrial function and/or mass. In each case, the

common factor that imparts this behavior is likely to be ATP depletion. This is supported by the slower rate of apoptosis following serum deprivation of *myc*−/− cells,[16,42] whose ATP depletion also likely arises from ETC dysfunction.[4] Mutations affecting these complexes are often associated with elevated ROS and ATP depletion and are commonly seen in inherited metabolic diseases and cancer.[30,31,33,56] Mutations in specific Complex V subunits such as MTATP6, or general reductions in Complex V, have also been described in cancer, often in association with ATP depletion and apoptotic resistance.[57,58]

Previous studies suggest that the initial stages of apoptosis and downstream components of the apoptotic machinery are ATP-dependent, including the activation of caspases 3 and 8, Apaf-1 and apoptosis-associated endonuclease.[44,45] As little as a 50% reduction in ATP levels can significantly delay apoptosis,[45] which is consistent with our finding that the apoptotic resistance of Drp1 cells can be reversed by activating AMPK and more than doubling ATP levels (Figure 8). AMPK activation has been reported to impart apoptotic resistance to a variety of cell types, although it is unclear as to whether this is due solely to the normalization of ATP levels.[59]

That Drp1 cells proliferate and survive offers strong evidence that small mitochondria *per se* are not themselves a direct trigger of apoptosis but rather require additional factors.[26] This is consistent with fission's central role during normal mitochondrial remodeling in proliferating cells where apoptosis would be an undesirable outcome. Fission is also required for the consumption of mitochondria during periods of starvation-induced autophagy, the purpose of which is to preserve cell viability by providing alternate energy sources.[20] Because apoptotic signaling is rapid and irreversible beyond a certain point,[16] it is not surprising that it is subject to multiple layers of regulation and that fission would not necessarily trigger an apoptotic response and might, in some cases, even block it.

In summary, our results demonstrate how defects in mitochondrial fission, ETC architecture and ATP production can conspire to promote survival in response to Myc deregulation.[31,52] Although Myc overexpression typically promotes mitochondrial biogenesis and ATP production,[4,15] it does so when essential nutrients and oxygen are abundant. When these become limiting due to poor vascular perfusion and loss of mitochondrial integrity, the attendant depletion of ATP may provide a buffer against the pro-apoptotic tendencies of Myc overexpression, thus favoring tumor cell survival.

Materials and Methods

Generation and maintenance of cell lines. Rat1a fibroblasts were routinely propagated in Dulbecco's modified Eagle's minimal essential medium (DMEM) supplemented with 10% fetal bovine serum, glutamine and penicillin/streptomycin as previously described.[7,14] Conditional Myc expression was achieved by stable transduction with the pBABE-puro-MycER retroviral vector (gift of Martin Eilers). Stable expression of the 710 amino-acid long variant 2 isoform of Drp1 (GenBank Accession No: NM_012063, Origene Technologies, Inc. Rockville, MD, USA) as a V5 epitope-tagged fusion protein was obtained in the pLenti6/V5 TOPO vector (Invitrogen, Inc., Carlsbad, CA). The cDNA was amplified using the forward PCR primer 5′-CACCATGGAGGCGCTAATTCCTGTC-3′ and the reverse primer 5′-CCAAAGATGAGTCTCCCGGATTTC-3′, where the underlined bases represent the initiation ATG and the penultimate codons, respectively. Following directional cloning, the orientation of the insert and its in-frame fusion to the V5 epitope coding region were confirmed by automated DNA sequencing. The Drp1-encoding vector, or an empty control vector, were then packaged according to the directions of the supplier and the resultant lentiviral stocks were used to transduce the above-described Rat1a-MycER cell line. Stable clones were selected in 2–5 μg/ml blasticidin, pooled for subsequent characterization and routinely maintained in blasticidin-containing medium. These cell lines are hereafter referred to as Drp1 cells and Vector cells. All retroviral and lentiviral work was approved by the University of Pittsburgh Institutional Biosafety Committee and was performed under BSL2+ conditions.

For confocal microscopic experiments, additional transfections were performed with the pEGFP-Mito and pDsRed2-Mito vectors (Clontech, Inc., Mountain View, CA, USA), which encode green and red fluorescent proteins, respectively, fused to the mitochondrial targeting sequence from subunit VIII of human cytochrome *c* oxidase. Cells were transfected with 1-2 μg of plasmid DNA using Superfect transfection reagent (Qiagen, Inc., Valencia, CA, USA), selected in 200 μg/ml of G-418 (Sigma-Aldrich, St. Louis, MO, USA) and isolated by fluorescence-activated cell sorting.

Confocal microscopy. Mitochondria were visualized in cells expressing pEGFP-Mito or pDsRed2-Mito vectors. Cells were grown to ~50% confluency in six-well, glass-bottom tissue culture plates. Fluorescent images of magnification ×20 were obtained with a Zeiss Axiovert fluorescent microscope (Wake Forest, NC, USA). Images of magnification ×60 were obtained on a Zeiss LSM710 confocal microscope (Wake Forest, NC, USA). Confocal stacks of the mitochondria were analyzed using Imaris software (Bitplane Scientific, South Windsor, CT, USA) and cellular 3D reconstructions were obtained as previously described.[4] Mean fluorescence intensities were obtained on at least 50 individual cells and quantified using ImageJ software (http://rsbweb.nih.gov/ij/). Live-cell confocal microscopy was performed on cells stained with MitoTracker Green FM at a concentration of 1 μM for 30 min before the start of experiment. Cells were counterstained with Hoechst 33342 at a concentration of 2 μg/ml. During the imaging, cells were maintained in phenol red-free DMEM in which the MitoTracker and Hoechst dyes were added at 1/10 the original concentration. Images were captured on the LSM710 microscope approximately every 45 s.

PEG-fusion assays. These were performed as described previously.[7] Briefly Vector and Drp1 cells expressing EGFP-Mito were co-plated with equal numbers of the same cells expressing DsRed2-Mito onto glass coverslips in 12-well plates. Following an overnight incubation, fresh medium containing cycloheximide (CHX; 30 μg/ml, Sigma-Aldrich) was added for 30 min to inhibit *de novo* synthesis of fluorescent proteins. The medium was then removed and 0.5 ml of 100% PEG 1500 (Sigma-Aldrich) was added for 1 min at room temperature. The coverslips were washed three times with DMEM + CHX, and subsequently incubated in the same medium for 2 h. The coverslips were then fixed for 30 min with ice-cold 3.7% para-formaldehyde in PBS, stained with DAPI and fixed onto glass microscope slides. A minimum of 20 heterokaryons were observed for each sample using confocal fluorescence microscopy as described above from which the percentage of co-localized (fused) mitochondria was calculated using the CoLocalizer Pro software (CoLocaliztion Research Software, Kochi, Japan) and expressed as the percentage of mitochondrial fusion.

Determination of mitochondrial mass and ROS. Mitochondrial mass was determined using MitoTracker Green FM and NAO. ROS levels were measured using CM-H2DCFDA and MitoSOX. All dyes were purchased from Life Technologies, Inc. (Carlsbad, CA, USA). Briefly, cells were seeded 1–2 days before staining and allowed to attain ~50% confluency unless otherwise stated. Adherent cells were exposed for 45 min to 500 nM MitoTracker Green FM, 2.5 μM of CM-H2DCFDA or 20 nM NAO in standard growth medium. In the case of MitoSOX, cells were exposed for 10 min to a 5-μM concentration of the dye. Immediately after exposure, adherent cells were trypsinized, titurated vigorously and then subjected to flow cytometric evaluation using a FACSCalibur flow cytometer (BD Biosciences, San Jose, CA, USA) as previously described.[7,14]

Measurements of OXPHOS and glycolysis. OXPHOS was quantified using a Seahorse Biosciences (North Billerica, MA, USA) XF24 Extracellular Flux Analyzer as previously described.[4,7] Briefly, 2×10^4 cells were seeded into individual wells of a 24-well plates and cultured overnight before assaying. Fresh medium was added and baseline O_2 consumption was quantified as a surrogate

measurement of OXPHOS. Several metabolic inhibitors were then added to determine the bioenergetic capacity of the mitochondria. These included: oligomycin, which blocks complex V and causes a build-up of protons across the inner mitochondrial matrix; FCCP, which causes protons exterior to the inner membrane to be carried across to the mitochondrial matrix; 2-DG), which inhibits glucose uptake for the initial step of glycolysis and reduces pyruvate transport into the TCA cycle; and rotenone, which inhibits Complex I and blocks both electron flow and oxygen consumption. Each point was determined from quadruplicate wells, and each experiment was performed at least twice. Glycolysis was quantified in parallel on the same samples by measuring the ECAR as previously described.[4,7]

ATP assay. ATP levels were measured using the ATPlite Luminescence Assay System (Perkin Elmer, Waltham, MA, USA) as previously described.[7] Briefly, 2×10^4 cells were seeded into individual wells of a 96-well plate and incubated overnight before assay, which was conducted on quadruplicate samples according to the directions of the supplier. The final calculated ATP levels were adjusted for slight variations in cell plating efficiencies ($<20\%$) based on cell counts performed on a parallel series of wells.

Western blotting. Western blotting of total cell lysates was performed as previously described.[7,14] The following primary antibodies were used: Anti-V5: 1:5000 (Invitrogen); anti-Sirt3: 1:1000 (Abcam, Cambridge, MA, USA), anti-Sirt5: 1:1000 (Abcam); anti-MFF: 1:1000 (Abcam); anti-MCAD: 1:2500; anti-cytochrome c: 1:1000 (Abcam); Anti-AMPK 1:2000 (Cell Signaling Technology, Beverley, MA, USA); Anti-phospho-AMPK (α-subunit Thr_{172}) 1:1000 (Cell Signaling Technology); anti β-actin: 1:10,000 (Santa Cruz, Santa Cruz, CA, USA). Horseradish peroxidase-tagged secondary antibodies were used at dilutions recommended by the supplier and included goat anti-mouse IgG:1 : 10 000 (Santa Cruz) and goat anti-rabbit IgG:1 : 5000 (Cell Signaling Technology). Blots were developed using the Pierce ECL Plus Western Blotting Substrate (Thermo Fisher Scientific, Inc., Waltham, MA, USA) as recommended by the supplier.

Cell sizing and apoptosis determinations. Monolayer cultures were trypsinized, washed twice in PBS and re-suspended in 1 ml of PBS. The average diameter of viable cells was then immediately determined with a Beckman-Coulter Cell Viability Analyzer (Beckman-Coulter, Inc., Indianapolis, IN, USA). Only cultures having a starting overall viability of $>90\%$ were analyzed. Diameters of at least 3000 viable cells/sample/day were determined on 3–5 individual samples measured on separate days. Apoptosis assays were also performed on the Cell Viability Analyzer by quantifying the fraction of trypan blue-positive cells in the combined floating and attached populations with each assay being performed in triplicate. These assays were in excellent agreement with parallel studies of Annexin V cell surface expression (not shown).[4,7]

Mitochondrial purification. Vector and Drp1 cells were harvested by trypsinization, combined with the non-adherent cell population and washed three times with PBS. The final pellets were re-suspended in 1 ml sucrose buffer (0.25 M sucrose; 10 mM Tris-HCl, pH 7.4; 1 mM EDTA and protease inhibitors) and disrupted using a cell homogenizer (Isobiotech, Heidelberg, Germany). The homogenates were then centrifuged at $100 \times g$ for 10 min, and the supernatants were re-centrifuged at $12\,000 \times g$ for 15 min. The supernatants containing cytoplasmic proteins were removed and saved. The mitochondria-enriched pellets were washed in the above sucrose buffer and saved. Protein concentrations in each fraction were then determined before SDS-PAGE and immunoblotting for cytochrome *c* as described above.

BNGE and *in situ* activity staining. Native ETC complexes were visualized by non-denaturing BNGE as described previously.[4] Briefly, isolated mitochondria were lysed by the addition of digitonin to a final ratio of 1 : 8 protein:digitonin and incubated on ice for 20 min. Coomassie blue solution (5% Coomassie blue G250 in 750 mM 6-aminocaproic acid) was added (1/20 v/v) followed by centrifugation at $14\,000 \times g$ for 20 min at 4 °C. The supernatant was then electrophoresed on a 3–12% Native PAGE Novex Bis-Tris gel (Invitrogen) in the buffer provided by the supplier, stained with Bio-Safe Coomassie G250 (Bio-Rad, Hercules, CA, USA) and de-stained with water. The gels were scanned and analyzed for band density using an AlphaEaseFC 2200 scanner and software (Alpha Innotech, Inc., San Leandro, CA, USA).

For Complex I activity measurements, the same blue-native gels used to quantify individual complexes were incubated at 37 °C for 1–2 h in 2 mM Tris-HCl, pH 7.4 buffer containing 2.5 mg/ml nitrotertrazolinum blue chloride and 0.1 mg/ml NADH. Densitometric analysis from triplicate gels was used to calculate the mean activity. Quantification of the ATPase activity of Complex V was performed by incubating gels at 37 °C for 3 h in 34 mM Tris-glycine, pH 7.8, 14 mM $MgSO_4$, 0.2% $Pb(NO_3)_2$ with freshly added 8 mM ATP. Bands were quantified as described for Complex I.

Conflict of Interest

The authors declare no conflict of interest.

Acknowledgements. We thank Michelle Barbi for assistance with metabolic Flux Analyzer studies and Maria Branca for help with confocal microscopy. This work was supported by NIH grants RO1 CA140624 to EVP, R01 DK090242 to ESG, R01 DK787775 to JV and Pennsylvania Department of Health, the PA CURE to BVH. JAG was supported by the Harold Amos Medical Faculty Development Program sponsored by the Robert Wood Johnson Foundation and a Hyundai Hope on Wheels Fellowship.

1. Gomez-Roman N, Felton-Edkins ZA, Kenneth NS, Goodfellow SJ, Athineos D, Zhang J *et al.* Activation by c-Myc of transcription by RNA polymerases I, II and III. *Biochem Soc Symp* 2006; **73**: 141–154.
2. Nesbit CE, Grove LE, Yin X, Prochownik EV. Differential apoptotic behaviors of c-myc, N-myc, and L-myc oncoproteins. *Cell Growth Differ* 1998; **9**: 731–741.
3. Dang CV, Le A, Gao P. MYC-induced cancer cell energy metabolism and therapeutic opportunities. *Clin Cancer Res* 2009; **15**: 6479–6483.
4. Graves JA, Wang Y, Sims-Lucas S, Cherok E, Rothermund K, Branca MF *et al.* Mitochondrial structure, function and dynamics are temporally controlled by c-Myc 2012*PLoS One* **7**: e37699.
5. Dang CV. Links between metabolism and cancer. *Genes Dev* 2012; **26**: 877–890.
6. Levine AJ, Puzio-Kuter AM. The control of the metabolic switch in cancers by oncogenes and tumor suppressor genes. *Science* 2010; **330**: 1340–1344.
7. Graves JA, Rothermund K, Wang T, Qian W, Van Houten B, Prochownik EV. Point mutations in c-Myc uncouple neoplastic transformation from multiple other phenotypes in rat fibroblasts. *PLoS One* 2010; **5**: e13717.
8. Morrish F, Isern N, Sadilek M, Jeffrey M, Hockenbery DM. c-Myc activates multiple metabolic networks to generate substrates for cell-cycle entry. *Oncogene* 2009; **28**: 2485–2491.
9. Vander Heiden MG, Cantley LC, Thompson CB. Understanding the Warburg effect: the metabolic requirements of cell proliferation. *Science* 2009; **324**: 1029–1033.
10. Wellen KE, Thompson CB. Cellular metabolic stress: considering how cells respond to nutrient excess. *Mol Cell* 2010; **40**: 323–332.
11. Fukumura D, Jain RK. Tumor microvasculature and microenvironment: targets for anti-angiogenesis and normalization. *Microvasc Res* 2007; **74**: 72–84.
12. Ji H, Wu G, Zhan X, Nolan A, Koh C, De Marzo A *et al.* Cell-type independent MYC target genes reveal a primordial signature involved in biomass accumulation. *PLoS One* 2011; **6**: e26057.
13. Iritani BM, Eisenman RN. c-Myc enhances protein synthesis and cell size during B lymphocyte development. *Proc Natl Acad Sci U S A* 1999; **96**: 13180–13185.
14. Rothermund K, Rogulski K, Fernandes E, Whiting A, Sedivy J, Pu L *et al.* C-Myc-independent restoration of multiple phenotypes by two C-Myc target genes with overlapping functions. *Cancer Res* 2005; **65**: 2097–2107.
15. Li F, Wang Y, Zeller KI, Potter JJ, Wonsey DR, O'Donnell KA *et al.* Myc stimulates nuclearly encoded mitochondrial genes and mitochondrial biogenesis. *Mol Cell Biol* 2005; **25**: 6225–6234.
16. Hoffman B, Liebermann DA. Apoptotic signaling by c-Myc. *Oncogene* 2008; **27**: 6462–6472.
17. Chan DC. Fusion and fission: interlinked processes critical for mitochondrial health. *Annu Rev Genet* 2012; **15**: 265–287.
18. Heath-Engel HM, Shore CC. Mitochondrial membrane dynamics, cristae remodelling and apoptosis. *Biochim Biophys Acta* 2006; **1763**: 549–560.
19. Huang P, Galloway CA, Yoon Y. Control of mitochondrial morphology through differential interactions of mitochondrial fusion and fission proteins. *PLoS One* 2011; **6**: e20655.
20. Okamoto K, Kondo-Okamoto N. Mitochondria and autophagy: critical interplay between the two homeostats. *Biochim Biophys Acta* 2012; **1820**: 595–600.
21. Estaquier J, Vallette F, Vayssiere JL, Mignotte B. The mitochondrial pathways of apoptosis. *Adv Exp Med Biol* 2012; **942**: 157–183.
22. Karbowski M. Mitochondria on guard: role of mitochondrial fusion and fission in the regulation of apoptosis. *Adv Exp Med Biol* 2010; **687**: 131–142.
23. Reddy PH, Reddy TP, Manczak M, Calkins MJ, Shirendeb U, Mao P. Dynamin-related protein 1 and mitochondrial fragmentation in neurodegenerative diseases. *Brain Res Rev* 2011; **67**: 103–118.

24. Smirnova E, Shurland DL, Ryazantsev SN, van der Bliek AM. A human dynamin-related protein controls the distribution of mitochondria. *J Cell Biol* 1998; **143**: 351–358.
25. Smirnova E, Griparic L, Shurland DL, van der Bliek AM. Dynamin-related protein Drp1 is required for mitochondrial division in mammalian cells. *Mol Biol Cell* 2001; **12**: 2245–2256.
26. Wasiak S, Zunino R, McBride HM. Bax/Bak promote sumoylation of DRP1 and its stable association with mitochondria during apoptotic cell death. *J Cell Biol* 2007; **177**: 439–450.
27. Friedman JR, Lackner LL, West M, DiBenedetto JR, Nunnari J, Voeltz GK. ER tubules mark sites of mitochondrial division. *Science* 2011; **334**: 358–362.
28. Littlewood TD, Hancock DC, Danielian PS, Parker MG, Evan GI. A modified oestrogen receptor ligand-binding domain as an improved switch for the regulation of heterologous proteins. *Nucleic Acids Res* 1995; **23**: 1686–16890.
29. Mateyak MK, Obaya AJ, Adachi S, Sedivy JM. Phenotypes of c-Myc-deficient rat fibroblasts isolated by targeted homologous recombination. *Cell Growth Differ* 1997; **8**: 1039–1048.
30. Lazarou M, Thorburn DR, Ryan MT, McKenzie M. Assembly of mitochondrial complex I and defects in disease. *Biochim Biophys Acta* 2009; **1793**: 78–88.
31. Lemarie A, Grimm S. Mitochondrial respiratory chain complexes: apoptosis sensors mutated in cancer? *Oncogene* 2011; **30**: 3985–4003.
32. Jonckheere AI, Smeitink JA, Rodenburg RJ. Mitochondrial ATP synthase: architecture, function and pathology. *J Inherit Metab Dis* 2012; **35**: 211–225.
33. Schon EA, Santra S, Pallotti F, Girvin ME. Pathogenesis of primary defects in mitochondrial ATP synthesis. *Semin Cell Dev Biol* 2001; **12**: 441–448.
34. Brand MD, Nicholls DG. Assessing mitochondrial dysfunction in cells. *Biochem J* 2011; **435**: 297–312.
35. Nicholls DG. Spare respiratory capacity, oxidative stress and excitotoxicity. *Biochem Soc Trans* 2009; **37**: 1385–1388.
36. Yadava N, Nicholls DG. Spare respiratory capacity rather than oxidative stress regulates glutamate excitotoxicity after partial respiratory inhibition of mitochondrial complex I with rotenone. *J Neurosci* 2007; **27**: 7310–7317.
37. Hardie DG, Ross FA, Hawley SA. AMPK: a nutrient and energy sensor that maintains energy homeostasis. *Nat Rev Mol Cell Biol* 2012; **13**: 251–262.
38. Murphy MP. How mitochondria produce reactive oxygen species. *Biochem J* 2009; **417**: 1–13.
39. Jastroch M, Divakaruni AS, Mookerjee S, Treberg JR, Brand MD. Mitochondrial proton and electron leaks. *Essays Biochem* 2010; **47**: 53–67.
40. Lempiäinen H, Shore D. Growth control and ribosome biogenesis. *Curr Opin Cell Biol* 2009; **21**: 855–863.
41. Evan GI, Wyllie AH, Gilbert CS, Littlewood TD, Land H, Brooks M *et al*. Induction of apoptosis in fibroblasts by c-myc protein. *Cell* 1992; **69**: 119–128.
42. Landay M, Oster SK, Khosravi F, Grove LE, Yin X, Sedivy J *et al*. Promotion of growth and apoptosis in c-myc nullizygous fibroblasts by other members of the myc oncoprotein family. *Cell Death Differ* 2000; **7**: 697–705.
43. Ow YP, Green DR, Hao Z, Mak TW. Cytochrome c: functions beyond respiration. *Nat Rev Mol Cell Biol* 2008; **9**: 532–542.
44. Eguchi Y, Srinivasan A, Tomaselli KJ, Shimizu S, Tsujimoto Y. ATP-dependent steps in apoptotic signal transduction. *Cancer Res* 1999; **59**: 2174–2181.
45. Leist M, Single B, Castoldi AF, Kühnle S, Nicotera P. Intracellular adenosine triphosphate (ATP) concentration: a switch in the decision between apoptosis and necrosis. *J Exp Med* 1997; **185**: 1481–1486.
46. Dagher Z, Ruderman N, Tornheim K, Ido Y. The effect of AMP-activated protein kinase and its activator AICAR on the metabolism of human umbilical vein endothelial cells. *Biochem Biophys Res Commun* 1999; **1265**: 112–115.
47. Germain M, Mathai JP, McBride HM, Shore GC. Endoplasmic reticulum BIK initiates DRP1-regulated remodelling of mitochondrial cristae during apoptosis. *EMBO J* 2005; **24**: 1546–1556.
48. Frank S, Gaume B, Bergmann-Leitner ES, Leitner WW, Robert EG, Catez F *et al*. The role of dynamin-related protein 1, a mediator of mitochondrial fission, in apoptosis. *Dev Cell* 2001; **1**: 515–525.
49. Lee YJ, Jeong SY, Karbowski M, Smith CL, Youle RJ. Roles of the mammalian mitochondrial fission and fusion mediators Fis1, Drp1, and Opa1 in apoptosis. *Mol Biol Cell* 2004; **15**: 5001–5011.
50. Szabadkai G, Simoni AM, Chami M, Wieckowski MR, Youle RJ, Rizzuto R. Drp1-dependent division of the mitochondrial network blocks intraorganellar Ca2 + waves and protects against Ca2 + -mediated apoptosis. *Mol Cell* 2004; **16**: 59–68.
51. Desagher S, Martinou JC. Mitochondria as the central control point of apoptosis. *Trends Cell Biol* 2000; **10**: 369–377.
52. Kwong JQ, Henning MS, Starkov AA, Manfredi G. The mitochondrial respiratory chain is a modulator of apoptosis. *J Cell Biol* 2007; **179**: 1163–1177.
53. Oster SK, Ho CS, Soucie EL, Penn LZ. The myc oncogene: MarvelouslY Complex. *Adv Cancer Res* 2002; **84**: 81–154.
54. Papanicolaou KN, Khairallah RJ, Ngoh GA, Chikando A, Luptak I, O'Shea KM *et al*. Mitofusin-2 maintains mitochondrial structure and contributes to stress-induced permeability transition in cardiac myocytes. *Mol Cell Biol* 2011; **31**: 1309–1328.
55. Bereiter-Hahn J, Vöth M, Mai S, Jendrach M. Structural implications of mitochondrial dynamics. *Biotechnol J* 2008; **3**: 765–780.
56. Nunnari J, Suomalainen A. Mitochondria: in sickness and in health. *Cell* 2012; **148**: 1145–1159.
57. Manfredi G, Fu J, Ojaimi J, Sadlock JE, Kwong JQ, Guy J *et al*. Rescue of a deficiency in ATP synthesis by transfer of MTATP6, a mitochondrial DNA-encoded gene, to the nucleus. *Nat Genet* 2002; **30**: 394–399.
58. Shidara Y, Yamagata K, Kanamori T, Nakano K, Kwong JQ, Manfredi G *et al*. Positive contribution of pathogenic mutations in the mitochondrial genome to the promotion of cancer by prevention from apoptosis. *Cancer Res* 2005; **65**: 1655–1663.
59. Dirks AJ, Hofer T, Marzetti E, Pahor M, Leeuwenburgh C, Mitochondrial DNA. mutations, energy metabolism and apoptosis in aging muscle. *Ageing Res Rev* 2006; **5**: 179–195.

Supplementary Information accompanies this paper on Cell Death and Disease website (http://www.nature.com/cddis)